SIAM J. SCI. COMPUT.
Vol. 27, No. 3, pp. 850–872

APPROXIMATION OF HYPERBOLIC MODELS FOR CHEMOSENSITIVE MOVEMENT*

FRANCIS FILBET† AND CHI-WANG SHU‡

Abstract. Numerical methods with different orders of accuracy are proposed to approximate hyperbolic models for chemosensitive movements. On the one hand, first- and second-order well-balanced finite volume schemes are presented. This approach provides exact conservation of the steady state solutions. On the other hand, a high-order finite difference weighted essentially nonoscillatory (WENO) scheme is constructed and the well-balanced reconstruction is adapted to this scheme to exactly preserve steady states and to retain high-order accuracy. Numerical simulations are performed to verify accuracy and the well-balanced property of the proposed schemes and to observe the formation of networks in the hyperbolic models similar to those observed in the experiments.

Key words. chemotaxis, hyperbolic systems, finite volume methods, finite difference methods, weighted essentially nonoscillatory schemes, well-balanced schemes

AMS subject classifications. 35L60, 92C15, 65M06

DOI. 10.1137/040604054

1. Introduction.

Chemosensitive movement is a process by which cells change their direction when reacting to the presence of a chemical substance, approaching chemically favorable environments, and avoiding unfavorable environments. In the biological literature there is a distinction between chemotaxis and chemokinesis. Chemokinesis describes nondirected bias in the movement behavior, which indirectly leads to an oriented movement of the population, whereas chemotaxis denotes a directed orientation toward or away from a chemical stimulus. However, from a modeling viewpoint this distinction is not necessary and we will summarize all these orientation effects in a chemosensitive movement.

In a simple situation, where we consider only cells and one chemical substance (the chemo-attractant), a model for the space and time evolution of the density $n = n(t,x)$ of cells and the chemical concentration $c = c(t,x)$ at time t and position $x \in \Omega \subset \mathbb{R}^d$ has been introduced by Patlak [19] and Keller and Segel [13]. This model assumes that the propagation of cells is performed via a diffusion process and reads

$$\frac{\partial n}{\partial t} - \operatorname{div}\left(\nabla n - n\,\chi'(c)\,\nabla c\right) = 0, \tag{1}$$

where $\chi'(c) \geq 0$ denotes the chemotactic sensitivity and the chemical concentration c is given either by the following parabolic equation describing the diffusion of the chemo-attractant created by the cells themselves:

$$\frac{\partial c}{\partial t} - D_c\,\Delta c = n - c, \tag{2}$$

*Received by the editors February 10, 2004; accepted for publication (in revised form) April 27, 2005; published electronically November 22, 2005.
http://www.siam.org/journals/sisc/27-3/60405.html

†Mathématiques et Applications, Physique Mathématique d'Orléans, CNRS UMR 6628, Université d'Orléans, B.P. 6759, F–45067 Orléans cedex 2, France (filbet@labomath.univ-orleans.fr).

‡Division of Applied Mathematics, Brown University, Providence, RI 02912 (shu@dam.brown.edu). This author's research was supported by ARO grants DAAD19-00-1-0405 and W911NF-04-1-0291, NSF grant DMS-0207451, and AFOSR grant F49620-02-1-0113.

with $D_c \geq 0$ denoting the motility (ability of the cell to move), or in the angiogenesis case, simply by

$$\frac{\partial c}{\partial t} = -c\, n. \tag{3}$$

However, this approach is not always sufficiently precise to describe the evolution of bacteria movements. Indeed, experiments show that bacteria such as *Escherichia coli* move along straight lines, suddenly stop to choose a new direction, and then continue moving in the new direction. This phenomenon, called run and tumble, can be modeled by a stochastic process called the velocity-jump process [10, 25]. A kinetic transport model for describing this velocity-jump process has been introduced in [18]. In fact, parabolic chemotaxis equations, such as the Patlak–Keller–Segel (PKS) model (1)–(2), have been obtained as the diffusion limit of this kinetic model, thus allowing the determination of the motility D_c and the chemotactic sensitivity χ' [10, 17]. A more recent tendency has been to use hyperbolic equations, which respect finite propagation speeds and are based on the individual movement patterns of the cells; see for instance [3, 4, 11, 21].

In this paper, we propose accurate numerical methods to approximate hyperbolic chemotaxis models. Our approach relies on finite volume schemes and finite difference schemes with high-order weighted essentially nonoscillatory (WENO) reconstructions and allows us to exactly preserve a particular class of steady state solutions.

The outline of this paper is as follows. In section 2, we present a hyperbolic system previously proposed in [21] to describe the early stages of the formation of blood vessels. In section 3, we first propose a first-order well-balanced (i.e., preserving exactly certain steady state solutions) finite volume scheme and then extend it to second-order accuracy. In section 4, we design a high-order well-balanced finite difference WENO scheme. Finally, in section 5 we perform numerical simulations of the nonlinear hyperbolic models of chemotaxis to verify accuracy and the well-balanced property of the proposed finite volume and high-order WENO finite difference schemes and to observe the formation of networks in the hyperbolic models similar to those observed in the experiments [4, 5, 21].

2. A hyperbolic model for chemotaxis. In this paper, we consider numerical approximations of a hyperbolic model introduced in [5, 21], in which the cell density $n(t,x)$ and the population flux $n\,u(t,x)$ are solutions of the hyperbolic system

$$\begin{cases} \dfrac{\partial n}{\partial t} + \operatorname{div}(n\,u) = 0, \\[2ex] \dfrac{\partial (n\,u)}{\partial t} + \operatorname{div}(n\ u \otimes u + P(n)) = n\,\chi'(c)\,\nabla c - \sigma\, n\ u, \end{cases} \tag{4}$$

where $P(n)$ is the pressure and σ is the friction coefficient. The evolution of the chemical concentration $c(t,x)$ is still given by (2).

This model is used to describe vasculogenesis (early formation of blood vessels) [5, 21] and can be recovered from a hydrodynamic scaling of a kinetic model [4]. Finite time blowup was proved in [14] for spherically symmetric solutions to the hyperbolic system (4) coupled with a Poisson-type equation to c,

$$-\Delta c = n.$$

Indeed, the Euler–Poisson system is widely studied in plasma physics and astrophysics to model star evolution and it is more expected that shock-type structures arise here,

which could explain why the singularities are not pointwise blow-up typical to the solution of the parabolic model (1) but are more like line concentrations (high concentrations along a line or curve). Such singularities are indeed observed in the numerical simulations in section 5 (formation of networks) and seem to be compatible with the experiments on endothelial cells [5, 21]. Moreover, the hyperbolic model (2), (4) admits an entropy inequality when $\chi(c) = c$, $P(n) = n$, and $D_c = 1$,

$$\frac{\partial \eta}{\partial t} + \operatorname{div} G = -\sigma n u^2 - \left(\frac{\partial c}{\partial t}\right)^2 \leq 0,$$

where

$$\begin{aligned} \eta(t,x) &= \eta_h(n, n\,u) - nc + \frac{1}{2}\left(c^2 + \left(\frac{\partial c}{\partial x}\right)^2\right), \\ G(t,x) &= G_h(n, n\,u) - nuc - \frac{\partial c}{\partial t}\frac{\partial c}{\partial x}, \end{aligned} \tag{5}$$

and (η_h, G_h) corresponds to the entropy pair for the homogeneous problem without the source term,

$$\eta_h(n, n\,u) = n(\log\, n - 1) + \frac{1}{2}\, n\, u^2, \qquad G_h(n, n\,u) = n\,u\left(\log n + \frac{1}{2}\, u^2\right). \tag{6}$$

Finally, we conclude this section with some remarks on the connection between the hyperbolic chemotaxis model (2)–(4) and the parabolic chemotaxis system (1)–(2). We first notice that, when $P(n) = n\,Id$, it is possible to recover (1) as the strong friction limit of (4), i.e., when σ goes to infinity. Moreover, the hyperbolic system (4) admits several types of steady state solutions, but the steady state solutions with a zero population flux ($nu = 0$) are particularly important since they are the same as those of the PKS model (1)–(2). Indeed, such steady state solutions satisfy

$$n\,\chi'(c)\,\nabla c - \nabla n = 0, \tag{7}$$

which is the equation satisfied by stationary solutions to the diffusive model for chemotaxis [17, 18].

In what follows, we restrict our attention to the one-dimensional case with $P(n) = n$:

$$\begin{cases} \dfrac{\partial n}{\partial t} + \dfrac{\partial (n\,u)}{\partial x} = 0, \\ \dfrac{\partial (n\ u)}{\partial t} + \dfrac{\partial}{\partial x}\left(n\ u^2 + n\right) = n\,\chi'(c)\dfrac{\partial c}{\partial x} - \sigma\ n\ u. \end{cases} \tag{8}$$

For future reference, we denote by U the unknown, by $F(U)$ the flux function, and by $S(U)$ the source term, which for the nonlinear system (8) are given by

$$U = \begin{pmatrix} n \\ n\,u \end{pmatrix}, \qquad F(U) = \begin{pmatrix} n\,u \\ n\,u^2 + n \end{pmatrix}, \qquad S(U) = \begin{pmatrix} 0 \\ n\,\chi'(c)\frac{\partial c}{\partial x} - \sigma\ n\ u \end{pmatrix}. \tag{9}$$

3. Finite volume approximations. Let us denote by $(x_{i-1/2})_{i\in\mathbb{Z}}$ a mesh of $\mathbb{R}$ and $x_i = (x_{i-1/2} + x_{i+1/2})/2$. Finite volume schemes for hyperbolic systems use an upwinding of the fluxes and in the semidiscrete case they provide a discretized version of (8) under the form

$$\Delta x_i \frac{d}{dt} U_i(t) + F_{i+1/2} - F_{i-1/2} = \Delta x_i \, S_i \tag{10}$$

where Δx_i denotes the mesh size $\Delta x_i = x_{i+1/2} - x_{i-1/2}$, and the discrete unknown $U_i(t)$ is

$$U_i(t) = \begin{pmatrix} n_i(t) \\ n_i(t)\, u_i(t) \end{pmatrix},$$

which represents an approximation to the cell-average of U in the cell $(x_{i-1/2}, x_{i+1/2})$. $F_{i+1/2}$ is an approximation of the flux at the point $x_{i+1/2}$ and S_i is an approximation of the cell-average of the source term $S(U)$ in the cell $(x_{i-1/2}, x_{i+1/2})$.

3.1. A first-order well-balanced scheme. In a basic first-order accurate scheme, the fluxes are classically computed as

$$F_{i+1/2} = \mathcal{F}(U_i(t), U_{i+1}(t)), \tag{11}$$

where the numerical flux $\mathcal{F}(U_i, U_{i+1})$ is computed via an approximation of the Riemann problem. We assume that the numerical flux $\mathcal{F}$ satisfies the following assumptions:

1. It is consistent with the physical flux:

$$\mathcal{F}(U, U) = F(U). \tag{12}$$

2. It preserves the nonnegativity of the density $n_i(t)$ for the homogeneous problem, namely, (8) without the source terms. That is, the scheme

$$\Delta x_i \frac{d}{dt} U_i(t) + F_{i+1/2} - F_{i-1/2} = 0, \tag{13}$$

where the numerical flux $F_{i+1/2}$ is defined by (11), maintains $n_i(t) \geq 0$ if $n_i(0) \geq 0$.

3. The scheme (13) with the numerical flux $F_{i+1/2}$ defined by (11) satisfies a cell entropy inequality for the entropy pair (6) for the homogeneous problem. According to [2], this means that we can find a numerical entropy flux $\mathcal{G}_h$ such that

$$\begin{aligned} &G_h(U_{i+1}) + \nabla_U \eta_h(U_{i+1}) \left(\mathcal{F}(U_i, U_{i+1}) - F(U_{i+1})\right) \\ &\qquad \leq \mathcal{G}_h(U_i, U_{i+1}) \leq G_h(U_i) + \nabla_U \eta_h(U_i) \left(\mathcal{F}(U_i, U_{i+1}) - F(U_i)\right), \end{aligned} \tag{14}$$

where $\nabla_U \eta_h$ is the derivative of η_h with respect to $U = \left(\begin{smallmatrix} n \\ nu \end{smallmatrix}\right)$.

Since the appearance of [7, 8], it has been known that cell-centered evaluations of the source term in a nonconservative hyperbolic system will generally not be able to preserve steady state solutions. In our case a particular class of steady state solutions, namely, the solution to (7), is given by

$$\log(n_i) - \chi(c_i) = \textit{constant}, \qquad u_i = 0 \qquad \forall\, i. \tag{15}$$

These steady state solutions play an important role in the modeling of chemosensitive movement because they also correspond to the steady state solutions of the parabolic equation (1), which describes the long time behavior of cells under the influence of the chemo-attractant c when the solutions do not blow up. Thus we would like to preserve these steady state solutions exactly at the discrete level.

Our approach follows the ideas of [1] for the shallow water equations (see also [6]). We propose a finite volume scheme according to (10) with flux functions

$$F_{i+1/2} = \mathcal{F}(U^-_{i+1/2}, U^+_{i+1/2}), \qquad U^\pm_{i+1/2} = \begin{pmatrix} n^\pm_{i+1/2} \\ n^\pm_{i+1/2}\, u^\pm_{i+1/2} \end{pmatrix}, \tag{16}$$

where the interface values $U^-_{i+1/2}$ and $U^+_{i+1/2}$ are locally reconstructed from U_i and U_{i+1}. The purpose of the reconstruction is not to increase the order of accuracy as usual, but to achieve a well-balanced property for the steady state solution (15). The source term is discretized by

$$S_i = \begin{pmatrix} 0 \\ \frac{1}{\Delta x_i}\left(n^-_{i+1/2} - n^+_{i-1/2}\right) \end{pmatrix} - \sigma \begin{pmatrix} 0 \\ n_i\, u_i \end{pmatrix}. \tag{17}$$

This ansatz is motivated by a balancing requirement. Indeed, when the population flux $n\,u$ is zero, the cell density n satisfies the balance of the momentum and the source term, i.e.,

$$\frac{\partial n}{\partial x} = n\,\chi'(c)\frac{\partial c}{\partial x}.$$

Integrating over $(x_{i-1/2}, x_{i+1/2})$, we obtain an approximation to the source term,

$$\frac{1}{\Delta x_i}\int_{x_{i-1/2}}^{x_{i+1/2}} n\,\chi'(c)\frac{\partial c}{\partial x}\,dx = \frac{1}{\Delta x_i}\left(n^-_{i+1/2} - n^+_{i-1/2}\right).$$

Therefore, when the velocity u is small, we are able to locally represent the cell-averaged source term as the discrete gradient of the momentum flux. This motivates the source term discretization (17). We will show later that this discretization is consistent with the source term in (8) also for solutions far away from these steady state solutions. It will be shown later that the steady state (15) is maintained exactly if, for such a state, we have

$$n^-_{i+1/2} = n^+_{i+1/2}, \qquad u^-_{i+1/2} = u^+_{i+1/2} = 0. \tag{18}$$

To achieve this, we choose

$$n^-_{i+1/2} = n_i\, e^{\chi_{i+1/2} - \chi(c_i)}, \qquad u^-_{i+1/2} = u_i \tag{19}$$

and

$$n^+_{i+1/2} = n_{i+1}\, e^{\chi_{i+1/2} - \chi(c_{i+1})}, \qquad u^+_{i+1/2} = u_{i+1}, \tag{20}$$

which lead to (18) for an arbitrary choice of $\chi_{i+1/2}$ when the steady state (15) is achieved. The evaluation of the interface value $\chi_{i+1/2}$ has to be such that the scheme is consistent and stable. We have chosen

$$\chi_{i+1/2} = \max\left(\chi(c_i), \chi(c_{i+1})\right) \tag{21}$$

in our numerical experiments. Another possible choice could be

$$\chi_{i+1/2} = \frac{1}{2}\left(\chi(c_i) + \chi(c_{i+1})\right).$$

To summarize, our first-order well-balanced finite volume scheme (10) is defined with the flux and reconstructions given by (16) and (19)–(20). The source term is given by (17), or equivalently, by

$$S_i = S^-_{i+1/2} + S^+_{i-1/2} - \sigma \begin{pmatrix} 0 \\ n_i u_i \end{pmatrix}, \tag{22}$$

with

$$S^-_{i+1/2} = \frac{1}{\Delta x_i}\begin{pmatrix} 0 \\ n^-_{i+1/2} - n_i \end{pmatrix}, \qquad S^+_{i-1/2} = \frac{1}{\Delta x_i}\begin{pmatrix} 0 \\ n_i - n^+_{i-1/2} \end{pmatrix}. \tag{23}$$

We may rewrite the scheme in a nonconservative form as in [2],

$$\Delta x_i \frac{d}{dt} U_i(t) + \mathcal{F}_l(U_i, U_{i+1}, c_i, c_{i+1}) - \mathcal{F}_r(U_{i-1}, U_i, c_{i-1}, c_i) = -\Delta x_i\, \sigma \begin{pmatrix} 0 \\ n_i u_i \end{pmatrix},$$

with the left and right numerical fluxes defined by

$$\begin{aligned} \mathcal{F}_l(U_i, U_{i+1}, c_i, c_{i+1}) &= F_{i+1/2} - \Delta x_i\, S^-_{i+1/2}, \\ \mathcal{F}_r(U_i, U_{i+1}, c_i, c_{i+1}) &= F_{i+1/2} + \Delta x_i\, S^+_{i+1/2}. \end{aligned} \tag{24}$$

Finally, the chemical concentration c is obtained by approximating (2) with a finite volume scheme,

$$\frac{dc_i}{dt} = \frac{D_c}{\Delta x_i}\left(\frac{c_{i+1} - c_i}{\Delta x_{i+1/2}} - \frac{c_i - c_{i-1}}{\Delta x_{i-1/2}}\right) + n_i - c_i, \tag{25}$$

where $\Delta x_{i+1/2} = x_{i+1} - x_i$.

We do not consider the influence of boundary conditions and will assume a periodic boundary condition. However, the numerical methods can be applied to general boundary conditions, as demonstrated in the numerical examples in section 5.

We have the following results for the scheme (10) defined above.

THEOREM 1. *The semidiscrete scheme* (10) *with* (16), (17), (19), *and* (20)

(i) *preserves the nonnegativity of* $n_i(t)$*;*
(ii) *preserves exactly the steady state given by* (15)*;*
(iii) *is consistent with the system* (8)*;*
(iv) *satisfies a cell entropy inequality associated with the entropy pair* (5) *when* $\chi(c_i) = c_i$ *and when* c_i *is given by the scheme* (25),

$$\Delta x_i \frac{\partial \eta_i}{\partial t} + G_{i+1/2} - G_{i-1/2} \le 0,$$

with

$$\eta_i = n_i\left(\log(n_i) - 1 + \frac{u_i^2}{2} - c_i\right) + \frac{1}{2}\left(c_i^2 + \frac{1}{\Delta x_i}\frac{(c_{i+1} - c_i)^2}{\Delta x_{i+1/2}}\right)$$

and a consistent numerical entropy flux $G_{i+1/2}$.

Proof. The ODE system (10) admits a unique smooth (in time) solution since the flux function is smooth enough. By this smoothness of the numerical solution in time, the flux $\mathcal{F}(U_l, U_r) = (\mathcal{F}_1, \mathcal{F}_2)(U_l, U_r)$ to the homogeneous problem (for example, the Lax–Friedrichs flux (41) to be used later) preserves the nonnegativity of n_i if and only if the first component of the flux $\mathcal{F}_1$ satisfies

$$\mathcal{F}_1((n_i = 0, u_i), (n_{i+1}, u_{i+1})) - \mathcal{F}_1((n_{i-1}, u_{i-1}), (n_i = 0, u_i)) \le 0 \quad \forall\, (u_j, n_j)_j. \tag{26}$$

Therefore, for our reconstruction (19)–(20), we need to check that, when $n_i = 0$,

$$\mathcal{F}_1(U^-_{i+1/2}, U^+_{i+1/2}) - \mathcal{F}_1(U^-_{i-1/2}, U^+_{i-1/2}) \le 0 \quad \forall\, u_{i-1}, u_i, u_{i+1}, n_{i-1}, n_{i+1}.$$

But, when $n_i = 0$, the reconstruction (19)–(20) gives that $n^+_{i-1/2} = n^-_{i+1/2} = 0$; hence,

$$\begin{aligned}
&\mathcal{F}_1(U^-_{i+1/2}, U^+_{i+1/2}) = \mathcal{F}_1((0, u_i), (n^+_{i+1/2}, u_{i+1})) \quad \forall\, (u_j, n^+_{j+1/2}, n^-_{j-1/2})_j,\\
&\mathcal{F}_1(U^-_{i-1/2}, U^+_{i-1/2}) = \mathcal{F}_1((n^-_{i-1/2}, u_{i-1}), (0, u_i)) \quad \forall\, (u_j, n^+_{j+1/2}, n^-_{j-1/2})_j.
\end{aligned}$$

Then from (26), we conclude that the scheme preserves nonnegativity of the density n_i.

To prove (ii), we assume the steady state (15) holds and would like to show

$$F_{i+1/2} - F_{i-1/2} = \Delta x_i\, S_i. \tag{27}$$

By the reconstruction of $n^+_{i+1/2}$ and $n^-_{i+1/2}$ given in (19)–(20), when (15) holds, we have

$$n^-_{i+1/2} = n^+_{i+1/2} = A\, e^{\chi_{i+1/2}}, \qquad u^-_{i+1/2} = u^+_{i+1/2} = 0,$$

where $A = n_i\, e^{-\chi(c_i)} = n_{i+1}\, e^{-\chi(c_{i+1})}$. On the one hand, the source term is given by

$$\Delta x_i\, S_i = \begin{pmatrix} 0 \\ n^-_{i+1/2} - n^+_{i-1/2} \end{pmatrix} = A \begin{pmatrix} 0 \\ e^{\chi_{i+1/2}} - e^{\chi_{i-1/2}} \end{pmatrix}. \tag{28}$$

On the other hand, by the consistency of the flux $\mathcal{F}$, we have

$$\begin{aligned}
F_{i+1/2} &= \mathcal{F}((A\, e^{\chi_{i+1/2}}, 0), (A\, e^{\chi_{i+1/2}}, 0))\\
&= F((A\, e^{\chi_{i+1/2}}, 0))\\
&= \begin{pmatrix} 0 \\ A\, e^{\chi_{i+1/2}} \end{pmatrix}.
\end{aligned} \tag{29}$$

Combining (28) and (29), we have proven (27).

To prove statement (iii), we apply the criterion in [1] and need to check two properties related to the consistency with the exact flux F and the consistency with the source term. The consistency with the exact flux is

$$\mathcal{F}_l(U, U, c, c) = \mathcal{F}_r(U, U, c, c) = F(U).$$

It is obviously satisfied since in this case $\chi_{i+1/2} = \chi(c)$, and therefore $n^+_{i+1/2} = n^-_{i+1/2} = n$. For the consistency with the source term, the criterion becomes

$$\mathcal{F}_r(U_l, U_r, c_l, c_r) - \mathcal{F}_l(U_l, U_r, c_l, c_r) = \begin{pmatrix} 0 \\ n\, \chi'(c)\, (c_r - c_l) + o(c_r - c_l) \end{pmatrix}, \tag{30}$$

as $U_r, U_l \to U = (n, u)$ and $c_r, c_l \to c$. In our case,

$$\mathcal{F}_r(U_l, U_r, c_l, c_r) - \mathcal{F}_l(U_l, U_r, c_l, c_r) = \begin{pmatrix} 0 \\ n_l\, e^{\chi_0 - \chi(c_l)} - n_l \end{pmatrix} - \begin{pmatrix} 0 \\ n_r\, e^{\chi_0 - \chi(c_r)} - n_r \end{pmatrix},$$

where $\chi_0 = \max(\chi(c_l), \chi(c_r))$. Now assume that $\chi_0 = \chi(c_l)$; then

$$\mathcal{F}_r(U_l, U_r, c_l, c_r) - \mathcal{F}_l(U_l, U_r, c_l, c_r) = \begin{pmatrix} 0 \\ n_r\, e^{-\chi(c_r)} \left(e^{\chi(c_r)} - e^{\chi(c_l)}\right) \end{pmatrix}$$

and we have

$$n_r\, e^{-\chi(c_r)} \left(e^{\chi(c_r)} - e^{\chi(c_l)}\right) = n\, e^{-\chi(c)} \left(e^{\chi(c_r)} - e^{\chi(c_l)}\right) + o(c_r - c_l),$$

which is consistent with the source term (30) since

$$n\, e^{-\chi(c)}\, \nabla e^{\chi(c)} = n\, \chi'(c)\, \nabla c.$$

The same argument applies when $\chi_0 = \chi(c_r)$, and we conclude that (30) always holds, which proves (iii).

In order to prove (iv), we proceed as in the continuous case and split the time derivative of the entropy into two pieces assuming $\chi(c) = c$,

$$\frac{\partial \eta_i}{\partial t} = \left(\frac{\partial \eta_{h,i}}{\partial t} - c_i \frac{\partial n_i}{\partial t}\right) + \left(-n_i \frac{\partial c_i}{\partial t} + \frac{1}{2}\left(\frac{\partial c_i^2}{\partial t} + \frac{1}{\Delta x_i} \frac{\partial}{\partial t} \frac{(c_{i+1} - c_i)^2}{\Delta x_{i+1/2}}\right)\right)$$

and we show that

$$\Delta x_i \left(\frac{\partial \eta_{h,i}}{\partial t} - c_i \frac{\partial n_i}{\partial t}\right) + G^1_{i+1/2} - G^1_{i-1/2} \le 0 \tag{31}$$

and

$$\Delta x_i \left(-n_i \frac{\partial c_i}{\partial t} + \frac{1}{2}\left(\frac{\partial c_i^2}{\partial t} + \frac{1}{\Delta x_i} \frac{\partial}{\partial t} \frac{(c_{i+1} - c_i)^2}{\Delta x_{i+1/2}}\right)\right) + G^2_{i+1/2} - G^2_{i-1/2} \le 0. \tag{32}$$

To prove (31), we first take notice of the assumption that the original numerical flux $\mathcal{F}$ satisfies a semidiscrete entropy inequality; hence (14) holds. Then, we set

$$G^1_{i+1/2} = \mathcal{G}_h(U^-_{i+1/2}, U^+_{i+1/2}) - \mathcal{F}_1(U^-_{i+1/2}, U^+_{i+1/2})\, c_{i+1/2}$$

and compute

$$\begin{aligned} G^1_{i+1/2} - G^1_{i-1/2} = {} & \mathcal{G}_h(U^-_{i+1/2}, U^+_{i+1/2}) - \mathcal{G}_h(U^-_{i-1/2}, U^+_{i-1/2}) \\ & - \mathcal{F}_1(U^-_{i+1/2}, U^+_{i+1/2})\, c_{i+1/2} + \mathcal{F}_1(U^-_{i-1/2}, U^+_{i-1/2})\, c_{i-1/2}. \end{aligned}$$

Using the two inequalities in (14), we get

$$\begin{aligned} G^1_{i+1/2} - G^1_{i-1/2} \le {} & G_h(U^-_{i+1/2}) + \nabla_U \eta_h(U^-_{i+1/2}) \left(\mathcal{F}(U^-_{i+1/2}, U^+_{i+1/2}) - F(U^-_{i+1/2})\right) \\ & - G_h(U^+_{i-1/2}) - \nabla_U \eta_h(U^+_{i-1/2}) \left(\mathcal{F}(U^-_{i-1/2}, U^+_{i-1/2}) - F(U^+_{i-1/2})\right) \\ & - \mathcal{F}_1(U^-_{i+1/2}, U^+_{i+1/2})\, c_{i+1/2} + \mathcal{F}_1(U^-_{i-1/2}, U^+_{i-1/2})\, c_{i-1/2}. \end{aligned}$$

This inequality can be rewritten as

$$\begin{aligned} G^1_{i+1/2} - G^1_{i-1/2} \leq & \left(\log(n^-_{i+1/2}) - \frac{1}{2}u_i^2 - c_{i+1/2}\right) \mathcal{F}_1(U^-_{i+1/2}, U^+_{i+1/2}) \\ & - \left(\log(n^+_{i-1/2}) - \frac{1}{2}u_i^2 - c_{i-1/2}\right) \mathcal{F}_1(U^-_{i-1/2}, U^+_{i-1/2}) \\ & + u_i \left(\mathcal{F}_2(U^-_{i+1/2}, U^+_{i+1/2}) - \mathcal{F}_2(U^-_{i-1/2}, U^+_{i-1/2}) + n^+_{i-1/2} - n^-_{i+1/2}\right). \end{aligned}$$

Now, by the definition of $n^-_{i+1/2}$, $n^+_{i-1/2}$, and S_i, we obtain

$$\begin{aligned} G^1_{i+1/2} - G^1_{i-1/2} \leq & \left(\log(n_i) - c_i - \frac{1}{2}u_i^2\right) \left(\mathcal{F}_1(U^-_{i+1/2}, U^+_{i+1/2}) - \mathcal{F}_1(U^-_{i-1/2}, U^+_{i-1/2})\right) \\ & + u_i \left(\mathcal{F}_2(U^-_{i+1/2}, U^+_{i+1/2}) - \mathcal{F}_2(U^-_{i-1/2}, U^+_{i-1/2}) \right. \\ & \left. + n^+_{i-1/2} - n^-_{i+1/2} + \sigma\, \Delta x_i n_i u_i\right) \\ \leq & -\Delta x_i\, \nabla_U \eta_h(U_i)\, \frac{dU_i}{dt} + \Delta x_i\, c_i\, \frac{dn_i}{dt}. \end{aligned}$$

We conclude that (31) holds.

To prove (32), we use the approximation (25) to the parabolic equation (2),

$$\begin{aligned} -n_i\, \frac{dc_i}{dt} &= -\left(\frac{dc_i}{dt} - \frac{1}{\Delta x_i}\, \left(\frac{c_{i+1}-c_i}{\Delta x_{i+1/2}} - \frac{c_i - c_{i-1}}{\Delta x_{i-1/2}}\right) + c_i\right)\, \frac{dc_i}{dt}, \\ &= -\left(\frac{dc_i}{dt}\right)^2 - \frac{1}{2}\, \frac{dc_i^2}{dt} + \frac{1}{\Delta x_i}\, \left(\frac{c_{i+1}-c_i}{\Delta x_{i+1/2}} - \frac{c_i - c_{i-1}}{\Delta x_{i-1/2}}\right)\, \frac{dc_i}{dt}. \end{aligned}$$

Using the equality

$$\begin{aligned} (c_{i+1} - c_i)\, \frac{d}{dt}\, \left(\frac{c_{i+1}-c_i}{\Delta x_{i+1/2}}\right) = & -\left(\frac{c_{i+1}-c_i}{\Delta x_{i+1/2}} - \frac{c_i - c_{i-1}}{\Delta x_{i-1/2}}\right)\, \frac{dc_i}{dt} \\ & + \left(\frac{c_{i+1}-c_i}{\Delta x_{i+1/2}}\, \frac{dc_{i+1}}{dt} - \frac{c_i - c_{i-1}}{\Delta x_{i-1/2}}\, \frac{dc_i}{dt}\right), \end{aligned}$$

we get

$$\frac{1}{2}\left(\frac{d}{dt}\frac{(c_{i+1}-c_i)^2}{\Delta x_{i+1/2}} + \Delta x_i \frac{dc_i^2}{dt}\right) - \Delta x_i\, n_i\, \frac{dc_i}{dt} + G^2_{i+1/2} - G^2_{i-1/2} \leq 0,$$

with

$$G^2_{i+1/2} = -\frac{c_{i+1}-c_i}{\Delta x_{i+1/2}}\, \frac{dc_{i+1}}{dt}.$$

Finally, gathering (31) and (32), we prove the result with $G_{i+1/2} = G^1_{i+1/2} + G^2_{i+1/2}$. ∎

Remark 1. When using the time-space fully discrete scheme

$$U_i^{k+1}-U_i^{k+1}+\frac{\Delta t}{\Delta x_i}\left(\mathcal{F}_l(U_i^k,U_{i+1}^k,c_i^k,c_{i+1}^k)-\mathcal{F}_r(U_{i-1}^k,U_i^k,c_{i-1}^k,c_i^k)\right)=-\Delta t\,\sigma\begin{pmatrix}0\\ n_i^k u_i^k\end{pmatrix},$$

the consistency and the well-balanced property are still valid. The stability is guaranteed under a CFL condition,

$$\sigma(U_i,U_{i+1})\Delta t\le\min(\Delta x_i,\Delta x_{i+1}),$$

where $\sigma(U_i,U_{i+1})\ge 0$ is a numerical speed at the interface (see [1, 2] for a detailed proof). Moreover, if we use a time explicit scheme to (25), we get a more restrictive condition on the time step

$$\Delta t\le\frac{\Delta x_i}{2}\,\min(\Delta x_{i-1/2},\Delta x_{i+1/2}).$$

3.2. Extension to a second-order approximation. Now we describe the extension to second-order accuracy. To this aim we reconstruct values at both sides of the interface. These new values are obtained in three steps: prediction of the gradients in each cell, linear extrapolation, and a limiting procedure to preserve nonnegativity. First, we compute two second-order accurate interface values $U_{i,r}$ and $U_{i+1,l}$ at the point $x_{i+1/2}$ from linear reconstructions in cells $(x_{i-1/2},x_{i+1/2})$ and $(x_{i+1/2},x_{i+3/2})$, respectively, following the three steps mentioned above. We remark that second-order accuracy is achievable only away from the vacuum $n_i=0$, since in the cell where $n_i=0$ the reconstructed linear function is flat to maintain the nonnegativity of n. Using the same reconstruction procedure, we also compute two interface values for the chemoattractant $e^{\chi(c)}$ at the point $x_{i+1/2}$, denoted by $(e^{\chi(c)})_{i,r}$ and $(e^{\chi(c)})_{i+1,l}$. Once these second-order reconstructed values are known, we further apply the reconstruction in the previous section to achieve well balancedness. This gives the second-order well-balanced scheme (10) with the flux defined by

$$F_{i+1/2}=\mathcal{F}(U_{i+1/2}^-,U_{i+1/2}^+)$$

and

$$U_{i+1/2}^-=\begin{pmatrix}n_{i+1/2}^-\\ n_{i+1/2}^-\,u_{i,r}\end{pmatrix},\qquad U_{i+1/2}^+=\begin{pmatrix}n_{i+1/2}^+\\ n_{i+1/2}^+\,u_{i+1,l}\end{pmatrix},\tag{33}$$

where $n_{i+1/2}^-$ and $n_{i+1/2}^+$ are given by

$$n_{i+1/2}^-=n_{i,r}\,\frac{(e^{\chi(c)})_{i+1/2}}{(e^{\chi(c)})_{i,r}},\qquad n_{i+1/2}^+=n_{i+1,l}\,\frac{(e^{\chi(c)})_{i+1/2}}{(e^{\chi(c)})_{i+1,l}},\tag{34}$$

with

$$(e^{\chi(c)})_{i+1/2}=\max\left((e^{\chi(c)})_{i,r},(e^{\chi(c)})_{i+1,l}\right).\tag{35}$$

The source term is computed as before at the interface,

$$S_i=S_{i+1/2}^-+S_i^c+S_{i-1/2}^+,\tag{36}$$

with

$$S^-_{i+1/2} = \frac{1}{\Delta x_i}\begin{pmatrix} 0 \\ n^-_{i+1/2} - n_{i,r} \end{pmatrix}, \qquad S^+_{i-1/2} = \frac{1}{\Delta x_i}\begin{pmatrix} 0 \\ n_{i,l} - n^+_{i-1/2} \end{pmatrix} \tag{37}$$

and

$$S^c_i = \frac{1}{\Delta x_i}\begin{pmatrix} 0 \\ \frac{1}{2}\left(\frac{n_{i,r}}{(e^{\chi(c)})_{i,r}} + \frac{n_{i,l}}{(e^{\chi(c)})_{i,l}}\right)\left((e^{\chi(c)})_{i,r} - (e^{\chi(c)})_{i,l}\right) \end{pmatrix} - \sigma \begin{pmatrix} 0 \\ n_i u_i \end{pmatrix}. \tag{38}$$

Using the definitions of the left and right numerical fluxes $\mathcal{F}_l$ and $\mathcal{F}_r$ in (24), a compact formulation of the scheme is

$$\Delta x_i \frac{d}{dt} U_i(t) + \mathcal{F}_l(U_{i,r}, U_{i+1,l}, c_{i,r}, c_{i+1,l}) - \mathcal{F}_r(U_{i-1,r}, U_{i,l}, c_{i-1,r}, c_{i,l}) = \Delta x_i \, S^c_i$$

and we prove the following result.

THEOREM 2. *Consider a numerical flux $\mathcal{F}$ (11) satisfying the first two assumptions: consistency (12) and maintenance of the nonnegavitity of $n_i(t)$ for (13). Moreover, assume the slope limiters used for the reconstruction of n ensure nonnegativity of n at the interfaces. Then, the scheme (33)–(38)*

(i) *preserves the nonnegativity of $n_i(t)$;*
(ii) *preserves exactly the steady state given by (15);*
(iii) *is consistent and second-order accurate with the system (8).*

Proof. We first prove (i). Assume that $n_i = 0$, which means that it is a local minimum of n. Since the linear reconstruction uses slope limiters to preserve nonnegativity of n, the reconstructed linear function in this cell is flat and we have $n_{i,r} = n_{i,l} = n_i = 0$ and $n^-_{i+1/2} = n^+_{i-1/2} = 0$. Therefore, we can apply the strategy of the proof of Theorem 1 to show the scheme preserves nonnegativity of $n_i(t)$.

To show that the steady state (15) is exactly maintained, we have to prove (27) when $n_i = A\, e^{\chi(c_i)}$ and $u_i = 0$ for all i with a constant A. To this aim, we observe that since the reconstruction procedure for n is the same as that for $e^{\chi(c)}$, we have

$$\frac{n_{i,r}}{(e^{\chi(c)})_{i,r}} = \frac{n_{i,l}}{(e^{\chi(c)})_{i,l}} = A \quad \forall\, i. \tag{39}$$

Of course we also have $u_{i,r} = u_{i,l} = 0$. On the one hand, we have

$$n^-_{i+1/2} = n^+_{i+1/2} = A\,(e^{\chi(c)})_{i+1/2},$$

which gives, by the consistency of the numerical flux,

$$F_{i+1/2} = \mathcal{F}(U^-_{i+1/2}, U^+_{i+1/2}) = F((A\,(e^{\chi(c)})_{i+1/2}, 0)) = \begin{pmatrix} 0 \\ A\,(e^{\chi(c)})_{i+1/2} \end{pmatrix}. \tag{40}$$

On the other hand, from (36) and (39) we also get

$$S_i = \frac{1}{\Delta x_i}\begin{pmatrix} 0 \\ n^-_{i+1/2} - n^+_{i-1/2} \end{pmatrix} = \frac{A}{\Delta x_i}\begin{pmatrix} 0 \\ (e^{\chi(c)})_{i+1/2} - (e^{\chi(c)})_{i-1/2} \end{pmatrix}.$$

Together with the expression (40), we have proved that the steady state (15) is exactly maintained at the discrete level.

To prove consistency, we apply the same technique as that in the proof of Theorem 1, whereas the second-order accuracy is easily obtained by observing that the well-balanced scheme is only a second-order perturbation of the second-order reconstruction. Moreover, the source term S_i^c is a second-order approximation of the source term $n\, e^{-\chi(c)}\, \nabla(e^{\chi(c(x))})$. □

It seems to be difficult to extend this method to higher than second-order accurate finite volume schemes because the well-balanced requirement induces constraints on the approximation of the source term. Moreover, in dimensions higher than one, finite volume schemes higher than second-order accurate are much more expensive in terms of computational cost than finite difference schemes. Therefore, in the next section we apply the well-balanced reconstruction to a high-order Lax–Friedrichs flux splitting finite difference WENO scheme, which does not have such an inconvenience.

4. Finite difference approximation. In this section we first briefly review some of the basics of the high-order finite difference approximation and the WENO reconstruction; for more details, see [12, 22]. We then adapt the well-balanced reconstruction to high-order finite difference WENO schemes. In this section we assume the mesh is uniform with mesh size Δx.

4.1. High-order finite difference WENO approximation for hyperbolic systems. A conservative finite difference spatial discretization to a hyperbolic system such as (4) approximates the derivative by a kth-order accurate conservative difference

$$\left.\frac{\partial F(U)}{\partial x}\right|_{x=x_i} = \frac{1}{\Delta x}\left(\hat{F}_{i+1/2} - \hat{F}_{i-1/2}\right) + O(\Delta x^k),$$

where $\hat{F}_{i+1/2}$ is the numerical flux, which typically is a Lipschitz continuous function of several neighboring values of $U = (n, nu)$. For the details of the numerical reconstruction of the flux $\hat{F}_{i+1/2}$ from the point values of $F(U)$, we refer to [12, 22]. Notice that the finite difference methods have the same format for one or more space dimensions, which is a major advantage in terms of accuracy and computational cost in dimensions higher than one.

In many applications the numerical flux $\hat{F}_{i+1/2}$ is obtained by the Lax–Friedrichs flux splitting

$$F^{\pm}(U) = \frac{1}{2}(F(U) \pm \alpha\, U), \qquad \alpha = \max_{m,U} |\lambda_m(U)|, \tag{41}$$

where $(\lambda_m(U))_m$ are the eigenvalues of the Jacobian $F'(U)$ and the maximum is taken over the relevant range of U. We will adopt this flux splitting in our scheme. The WENO procedure is used to reconstruct the numerical flux functions for $F^+(U)$ and $F^-(U)$ separately via upwinding.

For schemes higher than second-order accurate, the procedure should be carried out in local characteristic fields to avoid spurious oscillations. Thus one would first find an average $U_{i+1/2}$ of U_i and U_{i+1} (e.g., the Roe average [20], which exists for many physical systems), and then compute the left and right eigenvectors of the Jacobian $F'(U_{i+1/2})$ and put them into the rows of $R^{-1}_{i+1/2}$ and the columns of $R_{i+1/2}$, respectively, such that

$$R^{-1}_{i+1/2}\, F'(U_{i+1/2})\, R_{i+1/2} = \Lambda_{i+1/2},$$

where $\Lambda_{i+1/2}$ is a diagonal matrix containing the real eigenvalues of $F'(U_{i+1/2})$. One then transforms all the quantities needed for evaluating the numerical flux $\hat{F}_{i+1/2}$ to the local characteristic fields by left multiplying them with $R^{-1}_{i+1/2}$, and then computes the numerical fluxes by the scalar procedure in each characteristic field. Finally, the flux in the original physical space is obtained by left multiplying by $R_{i+1/2}$ the numerical flux obtained in the local characteristic fields.

We refer to [12, 22] for more details on WENO schemes and conservative finite difference methods.

4.2. A well-balanced reconstruction. In this section, we describe the strategy for obtaining a kth-order well-balanced finite difference WENO scheme for arbitrary k. From the previous description, we have constructed a numerical flux using the characteristic Lax–Friedrichs flux splitting and obtained a kth-order approximation of the flux $\hat{F}_{i+1/2}$ via WENO reconstruction. Then, we have

$$\hat{F}_{i+1/2} = \hat{F}^+_{i+1/2} + \hat{F}^-_{i+1/2},$$

with

$$\hat{F}^+_{i+1/2} = R_{i+1/2}\left(R^{-1}_{i+1/2}\left(F(U) + \alpha U\right)\right)_{i,r}, \tag{42}$$

$$\hat{F}^-_{i+1/2} = R_{i+1/2}\left(R^{-1}_{i+1/2}\left(F(U) - \alpha U\right)\right)_{i+1,l}, \tag{43}$$

where $(\cdot)_{i,r}$ and $(\cdot)_{i+1,l}$ denote high-order WENO reconstructions at the cell boundary $x_{i+1/2}$ from the cells $(x_{i-1/2}, x_{i+1/2})$ and $(x_{i+1/2}, x_{i+3/2})$, respectively.

We now modify the numerical flux $\hat{F}^{\pm}_{i+1/2}$ to achieve the well-balanced property. The well-balanced finite difference scheme approximating (8) has the form

$$\Delta x \frac{d}{dt} U_i(t) + F_{i+1/2} - F_{i-1/2} = n_i\, e^{-\chi(c_i)} \begin{pmatrix} 0 \\ S_{i+1/2} - S_{i-1/2} \end{pmatrix} - \sigma \begin{pmatrix} 0 \\ n_i\, u_i \end{pmatrix}, \tag{44}$$

where $S_{i+1/2} - S_{i-1/2}$ is a conservative finite difference approximation to $\Delta x\, \partial_x e^{\chi(c)}$. Indeed, from the points values $S_i = e^{\chi(c_i)}$, we can reconstruct two kth-order accurate WENO or ENO [24] fluxes $S_{i+1/2}$, one from the interval $(x_{i-1/2}, x_{i+1/2})$ denoted by $S_{i,r}$ (the same reconstruction procedure used for computing $\hat{F}^+_{i+1/2}$), and the other from the interval $(x_{i+1/2}, x_{i+3/2})$ denoted by $S_{i+1,l}$ (the same reconstruction procedure used for computing $\hat{F}^-_{i+1/2}$). Finally, we choose, for instance,

$$S_{i+1/2} = \max\left(S_{i,r}, S_{i+1,l}\right). \tag{45}$$

Now, the numerical flux $F_{i+1/2}$ for the well-balanced scheme (44) is constructed from the following perturbation from the classical WENO flux $\hat{F}_{i+1/2}$:

$$F^+_{i+1/2} = \hat{F}^+_{i+1/2}\, \frac{S_{i+1/2}}{S_{i,r}}, \qquad F^-_{i+1/2} = \hat{F}^-_{i+1/2}\, \frac{S_{i+1/2}}{S_{i+1,l}}. \tag{46}$$

For this algorithm, we prove the following result.

THEOREM 3. *Consider the Lax–Friedrichs flux splitting scheme coupled with the kth-order ENO or WENO reconstruction for the homogeneous problem* (8). *Then, the scheme* (44)–(46)

(i) *preserves the steady state given by* (15) *for the ENO reconstruction, and for the WENO reconstruction it preserves this steady state up to the parameter* ε*, which is used in the smooth indicator to avoid having the denominator become zero and which typically takes the value* $\varepsilon = 10^{-6}$ [12];

(ii) *is kth-order accurate with the system* (8).

Proof. We first prove (i). Assume that the steady state (15) is achieved,

$$n_i = A\, e^{\chi(c_i)}, \quad u_i = 0 \quad \forall\, i.$$

Then, for such a discrete solution $U_i = (n_i, u_i)$ the Lax–Friedrichs flux splitting is computed as

$$R^{-1}_{i+1/2} = \begin{pmatrix} 1 & 1 \\ -1 & 1 \end{pmatrix}, \qquad R_{i+1/2} = \begin{pmatrix} 1/2 & -1/2 \\ 1/2 & 1/2 \end{pmatrix},$$

which do not vary with i. This leads to

$$\Big(R^{-1}_{i+1/2}\,(\,F(U) + \alpha\, U\,)\Big)_{i,r} = \left(n \begin{pmatrix} 1+\alpha \\ 1-\alpha \end{pmatrix}\right)_{i,r},$$
$$\Big(R^{-1}_{i+1/2}\,(\,F(U) - \alpha\, U\,)\Big)_{i+1,l} = \left(n \begin{pmatrix} 1-\alpha \\ 1+\alpha \end{pmatrix}\right)_{i+1,l}.$$

Now we use the property of the ENO reconstruction [24] that for any constant λ,

$$(\lambda\, n)_{i,r} = \lambda\,(n)_{i,r}, \qquad (\lambda\, n)_{i+1,l} = \lambda\,(n)_{i+1,l}, \tag{47}$$

whereas for the WENO reconstruction,

$$(\lambda\, n)_{i,r} = \lambda\,(n)_{i,r} + O(\varepsilon), \qquad (\lambda\, n)_{i+1,l} = \lambda\,(n)_{i+1,l} + O(\varepsilon),$$

where ε is the small parameter used in the smooth indicator to avoid having the denominator become zero and typically takes the value $\varepsilon = 10^{-6}$ [12]. From now on we will use (47) in the analysis. Then, we get

$$\Big(R^{-1}_{i+1/2}\,(\,F(U) + \alpha\, U\,)\Big)_{i,r} = \begin{pmatrix} 1+\alpha \\ 1-\alpha \end{pmatrix} n_{i,r},$$
$$\Big(R^{-1}_{i+1/2}\,(\,F(U) - \alpha\, U\,)\Big)_{i+1,l} = \begin{pmatrix} 1-\alpha \\ 1+\alpha \end{pmatrix} n_{i+1,l}.$$

When the steady state (15) is achieved, the classical finite difference flux is given by

$$\hat{F}^{+}_{i+1/2} = n_{i,r} \begin{pmatrix} \alpha \\ 1 \end{pmatrix}, \qquad \hat{F}^{-}_{i+1/2} = n_{i+1,l} \begin{pmatrix} -\alpha \\ 1 \end{pmatrix}.$$

On the one hand, when the steady state (15) is reached, we know that

$$n_i = A\, e^{\chi(c_i)} \quad \forall\, i,$$

and since the reconstruction procedures for n and $e^{\chi(c)}$ are identical (using WENO or ENO reconstruction), we have

$$\hat{F}^{+}_{i+1/2} = A \begin{pmatrix} \alpha \\ 1 \end{pmatrix} S_{i,r}, \qquad \hat{F}^{-}_{i+1/2} = A \begin{pmatrix} -\alpha \\ 1 \end{pmatrix} S_{i+1,l}.$$

Then, by the definition of $F^{\pm}_{i+1/2}$ in (46), we get

$$F_{i+1/2} = A \begin{pmatrix} 0 \\ 1 \end{pmatrix} S_{i+1/2}.$$

On the other hand, by the construction of the source term (44),

$$S_i = n_i\, e^{-\chi(c_i)} \begin{pmatrix} 0 \\ 1 \end{pmatrix} \left(S_{i+1/2} - S_{i-1/2}\right).$$

When the steady state (15) is reached, we have $n_i\, e^{-\chi(c_i)} = A$ for all i; hence,

$$S_i = A \begin{pmatrix} 0 \\ 1 \end{pmatrix} (S_{i+1/2} - S_{i-1/2}),$$

which exactly satisfies the balance with the flux difference $F_{i+1/2} - F_{i-1/2}$.

Now let us prove (ii); i.e., the numerical scheme is a kth-order approximation to (8). The source term can be written in the form

$$n\,\chi'(c)\frac{\partial c}{\partial x} = n\, e^{-\chi(c)}\, \frac{\partial}{\partial x} e^{\chi(c)}$$

and clearly the right-hand side of (44) is a kth-order approximation to this source term when the flux $S_{i+1/2}$ is defined by (45), since both $S_{i,r}$ and $S_{i+1,l}$ are kth-order fluxes computed by WENO reconstruction. Also, it is obvious that $F^{\pm}_{i+1/2}$ is only a kth-order perturbation of the original kth-order accurate WENO flux $\hat{F}^{\pm}_{i+1/2}$, since the difference between $S_{i,r}$ and $S_{i+1,l}$ is at the level of truncation error for the kth-order WENO reconstruction. This demonstrates that the scheme (44) is kth-order accurate. ∎

5. Numerical simulations.

5.1. Accuracy test in one dimension. In this example, we consider the one-dimensional hyperbolic system (8) with $\chi'(c) = \frac{1}{1+c}$,

$$\begin{cases} \dfrac{\partial n}{\partial t} + \dfrac{\partial (nu)}{\partial x} = 0, \\ \dfrac{\partial (nu)}{\partial t} + \dfrac{\partial}{\partial x}\left(nu^2 + n\right) = \dfrac{n}{1+c}\,\dfrac{\partial c}{\partial x} - \sigma\, nu. \end{cases} \tag{48}$$

We take periodic boundary conditions, $\sigma = 1$, $t \in [0, T_{end}]$, with $T_{end} = 1$ and smooth initial data

$$n(0,x) = 1 \,+\, 0.2\,\cos(\pi\, x), \quad u(0,x) = 0, \quad x \in [-1,1],$$

whereas the chemo-attractant c is fixed to

$$c(x) = \exp(-16\, x^2), \quad x \in [-1,1].$$

This system does not admit an explicit solution, but to evaluate the error and the order of accuracy we first compute an accurate approximation using the fifth-order accurate classical WENO scheme with 1600 points and compare different numerical solutions with this reference solution. To show the advantage of the well-balanced

TABLE 1
Comparison of L^1 errors and numerical orders of accuracy for the classical WENO scheme and well-balanced WENO scheme with fourth-order Runge–Kutta time discretization.

Number of points	WENO		Well-balanced WENO	
	L^1 error	order	L^1 error	order
50	1.21E-04		7.90E-05	
100	5.86E-06	4.37	3.69E-06	4.42
200	4.00E-07	3.87	2.22E-07	4.05
400	2.00E-08	4.32	1.27E-08	4.13

TABLE 2
Comparison of L^1 errors and numerical orders of accuracy for a second-order finite volume scheme and well-balanced finite volume scheme with second-order Runge–Kutta time discretization.

Number of points	Finite volume		Well-balanced finite volume	
	L^1 error	order	L^1 error	order
50	1.13E-02		8.01E-03	
100	2.94E-03	1.94	2.30E-03	1.80
200	7.74E-04	1.92	6.01E-04	1.94
400	2.01E-04	1.94	1.58E-04	1.93

algorithm, we compare a fifth-order WENO finite difference scheme with and without the well-balanced reconstruction (presented in section 4) coupled with a fourth-order Runge–Kutta scheme for the time discretization.

In Table 1, we present the L^1 errors and numerical orders of accuracy obtained from both schemes. We observe that both methods achieve orders of accuracy above four and the well-balanced approach not only preserves the high-order accuracy, but also in this case allows us to reduce the error even if the solution is far from the equilibrium. We also give in Table 2 the L^1 errors and numerical orders of accuracy for the second-order finite volume monotone upstream-centered scheme for conservation laws (MUSCL) [16], namely, a linear reconstruction based on the usual minmod limiters,

$$\text{minmod}(a,b) = \frac{sign(a) + sign(b)}{2} \min(|a|, |b|),$$

the Lax–Friedrichs monotone numerical flux, and the second-order TVD time discretization [23], with and without the well-balanced reconstruction presented in section 3. Second order is well achieved but the numerical errors are large compared to those obtained from the WENO scheme on the same mesh.

To test the steady state conservation, we consider the steady state solution

$$n_0(x) = (1 + c(x))/10, \quad u(0,x) = 0, \tag{49}$$

where c is given by

$$c_0(x) = \begin{cases} 1 & \text{if } |x| \le 1/2, \\ 0.125 & \text{else.} \end{cases} \tag{50}$$

We compute the numerical solution using the WENO scheme with and without the well-balanced reconstruction and observe that the density n and the population flux nu are exactly conserved up to the round-off error with the well-balanced reconstruction, whereas spurious oscillations are generated when a centered approximation of

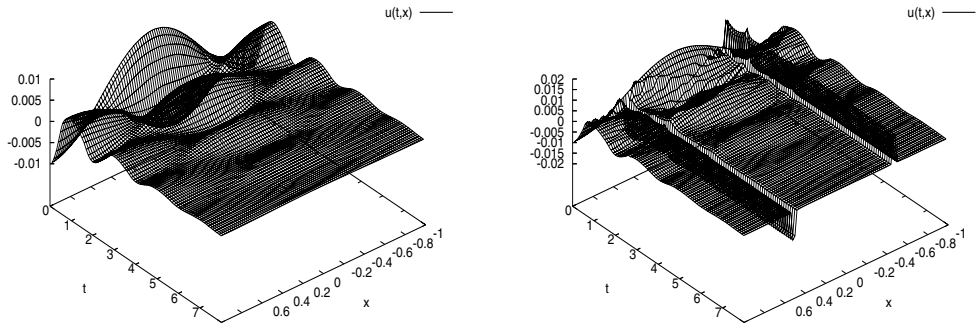

FIG. 1. *Accuracy test for well-balanced steady state resolution: time evolution of the population flux $n(t,x)\ u(t,x)$. Left: WENO scheme with the well-balanced reconstruction. Right: WENO schemes with a centered approximation of the source term.*

the source term is used. In Figure 1, we also present the numerical results obtained for a perturbation of the steady state: $n(t=0,x)$ and $c(t=0,x)$ are given by (49)–(50) and

$$u(t,x) = 0.01\,\cos(\pi x), \quad x \in [-1,1].$$

Then, some spurious oscillations appear in the population flux close to the discontinuities of the source term c when a centered approximation to the source term is used.

5.2. Convergence to the equilibrium in one dimension. Now we perform numerical simulations using the well-balanced fifth-order WENO finite difference scheme to observe the long time behavior of the solution to the hyperbolic model (48) with $\sigma = 0.25$ and $x \in [-6,6]$ with periodic boundary conditions, with the chemo-attractant c being the solution of the parabolic equation

$$\begin{cases} \dfrac{\partial c}{\partial t} - \dfrac{1}{10}\dfrac{\partial^2 c}{\partial x^2} = \alpha\, n - c, \\ \\ c(t,-6) = c(t,6) = 0, \end{cases}$$

and α a given compactly supported function

$$\alpha(x) = \begin{cases} (16-x^2)/16 & \text{if } |x| \le 4, \\ 0 & \text{else.} \end{cases}$$

The initial density is chosen as a constant density $n = 1$, whereas the initial population flux $n\ u$ and chemo-attractant c are equal to zero.

To observe the convergence to an equilibrium state we plot in Figure 2 the evolution of the L^1 norm of the time derivative of the cell density $\partial_t n$. We also plot the evolution of the cell density on different time intervals and at the final time ($t = 200$) when the steady state is reached. Clearly, the curves at $t = 25$ and $t = 200$ are overlapping, indicating that the numerical solution has already converged to steady state by visual inspection at $t = 25$.

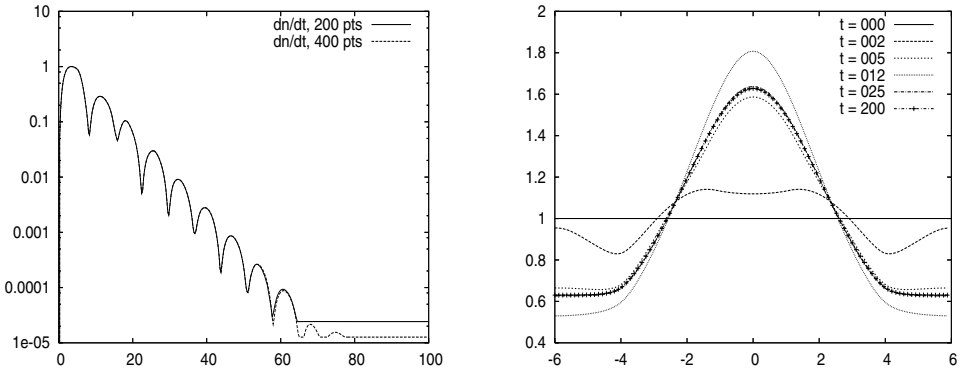

(a) (b)

FIG. 2. *Convergence to equilibrium.* (a) *Time evolution of the* L^1 *norm of the time derivative of the cell density* $\partial_t n(t,x)$. (b) *Time evolution of the cell density* $n(t,x)$ *for* $t = 0$, 2, 5, 12, 25, *and* 200.

5.3. Chemosensitive movement in two dimensions. In the previous two numerical examples, we have shown the efficiency of the finite difference WENO method for treating the convergence to steady states and the evolution of the cell density. Now we present numerical simulations obtained with the well-balanced fifth-order (in space) finite difference method to show that the hyperbolic models can give a good description of cell motion.

We consider the system in two space dimension,

$$\begin{cases} \dfrac{\partial n}{\partial t} + \operatorname{div}(nu) = 0, \\ \dfrac{\partial (nu)}{\partial t} + \operatorname{div}\left(nu \otimes u + n\right) = n\,\nabla c - \sigma\, nu, \end{cases}$$

where $\sigma = 0$ and the chemo-attractant c is fixed and concentrated at the origin (0,0),

$$c(x) = 400\, \exp(-x^2)/\pi, \quad x \in [0,2]^2.$$

We then consider two cell concentrations located far from the high concentration regions of the chemo-attractant. In Figure 3, we represent the evolution of cells, which move and stretch to the highest concentration region of the chemo-attractant. This simple test illustrates the attractive effect of the chemo-attractant gradient on the population flux nu and on the cell density n.

5.4. Formation of networks. As in [21, 5], we perform numerical simulations of the hyperbolic model (4) coupled with (2) on a square box of length $L = 20$ with periodic boundary conditions. For good accuracy, we use the well-balanced fifth-order WENO scheme described in the previous section to approximate the solution of (4) and a fourth-order finite difference scheme to approximate the solution of the parabolic equation (2),

$$\frac{dc_i}{dt} = D_c\, \frac{(-c_{i+2} + 16c_{i+1} - 30c_i + 16c_{i-1} - c_{i-2})}{12\Delta x^2} + n_i - c_i.$$

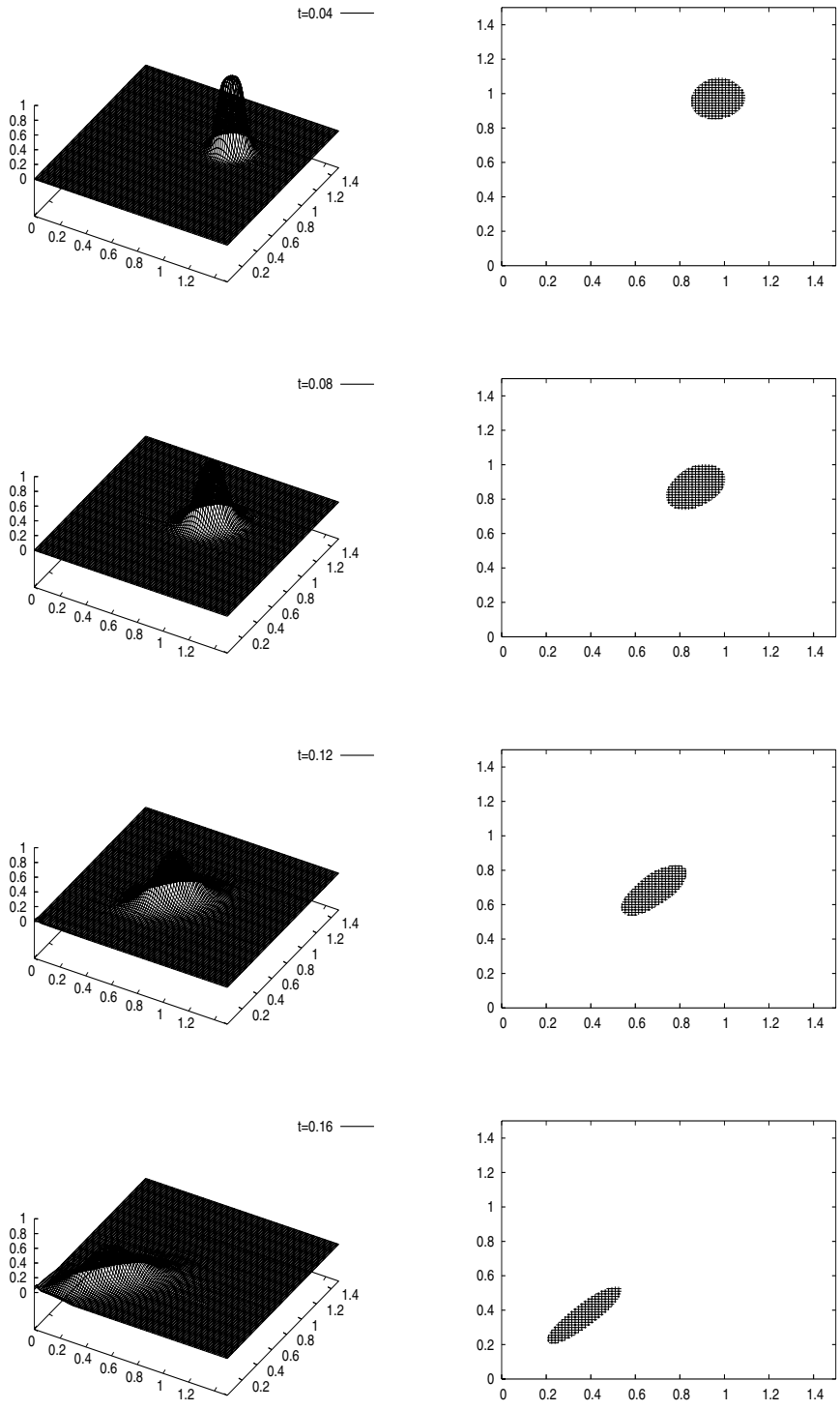

FIG. 3. *Chemosensitive movement: Time evolution of the cell density* $n(t,x)$ *at time* $t = 0.04$, 0.08, 0.12, *and* 0.16.

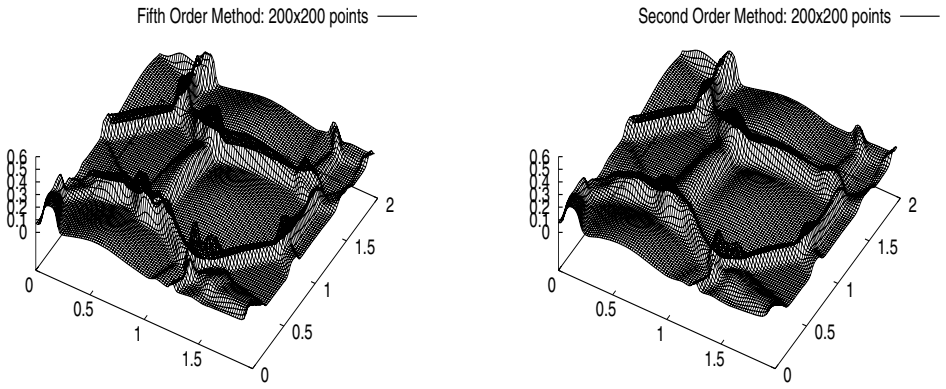

(a) (b)

FIG. 4. *Formation of network: comparison of numerical results between* (a) *the fifth-order WENO method and* (b) *the second-order finite volume scheme with* 200^2 *grid points.*

These results can be compared with those obtained in [4, 5] for the formation of networks: high cell concentrations are generated and linked together by line concentrations.

In (2) we take the diffusion rate $D_c = 1/10$ and also in (4) choose the pressure to be

$$P(n) = \beta\, n,$$

where $\beta = 1/4$ is the mean cell radius, $\chi'(c) = 1$, and the friction is $\sigma = 1/10$.

Now, the initial datum $n(0)$ is chosen by throwing cells randomly inside the box, with zero population flux $nu(0) = 0$ and zero concentration $c(0) = 0$ initially. More precisely, for $(x, y) \in (0, L)^2$, we choose

$$n(0, x, y) = \frac{1}{(2\,\pi\sigma)^2} \sum_{i=1}^{N} \exp\left(\frac{-\left((x - x_i)^2 + (y - y_i)^2\right)}{2\,\sigma^2} \right),$$

where $(x_i, y_i)_{1 \le i \le N}$ are uniformly distributed random variables in the box $(0, L)^2$, each Gaussian bump of width σ representing a single cell. Thus N denotes the total number of cells.

We first present a comparison between the fifth-order finite difference scheme and the second-order finite volume method to show the advantage of the high-order method. In Figure 4, we give the cell density on the square $[0, 2] \times [0, 2]$ at time $t = 0.31$ obtained with 200^2 points using the two methods. We can observe that the network is formed for both methods, but the numerical diffusion of the second-order finite volume scheme is more noticeable. We also present the cell density at time $t = 0.31$ and $x = -1.24$ for different meshes: 200^2 and 400^2 grid points for the fifth-order method, and 200^2, 400^2, and 800^2 points for the second-order method, in Figure 5. Clearly, the fifth-order WENO scheme gives results that converge faster and are more accurate than the finite volume scheme used in [4]. Even with 800^2 points, the numerical solution obtained with the second-order scheme still does not

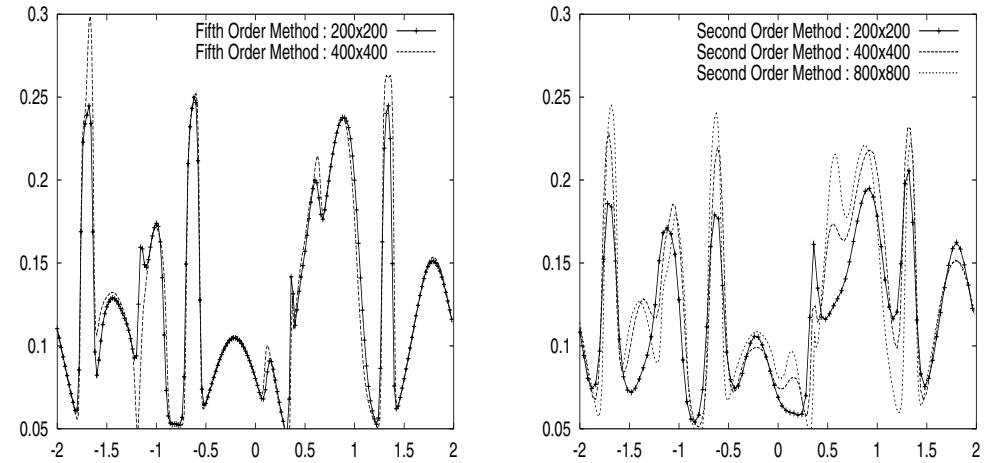

FIG. 5. *Formation of network: comparison of numerical results between* (a) *the fifth-order WENO method with* 200^2 *and* 400^2 *grid points and* (b) *the second-order finite volume scheme with* 200^2, 400^2, *and* 800^2 *grid points. Density cut at* $x = -1.24$.

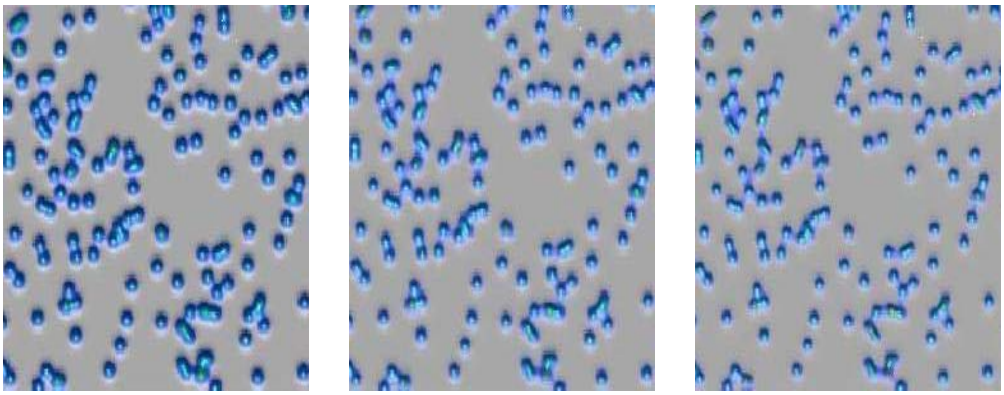

FIG. 6. *Formation of network: time evolution* ($t = 0.20$, 0.26, *and* 0.33) *of the cell density with* $N = 400$.

seem to be of the quality of the solution obtained with the fifth-order one using only 200^2 points, in terms of capturing the complicated features in the solution.

Finally, we present different numerical simulations when the initial total cell density N varies. Figures 6 and 7 represent a zoom of the cell density evolution for different initial concentrations ($N = 400$, 800, and 1200). On the one hand, in Figure 6 we observe the formation of high concentration regions but the number of cells is not large enough to generate a network. Indeed, a local density (representing several cells) does not interact with the surrounding densities; then local high concentrations are produced without any link to other cell densities. On the other hand, in Figure 7, cells are first uniformly located and then move to generate high concentration regions which are linked together by chords representing cells which are stretching. Finally, a network is formed as observed in the experiments [4, 21]. We cannot interpret the

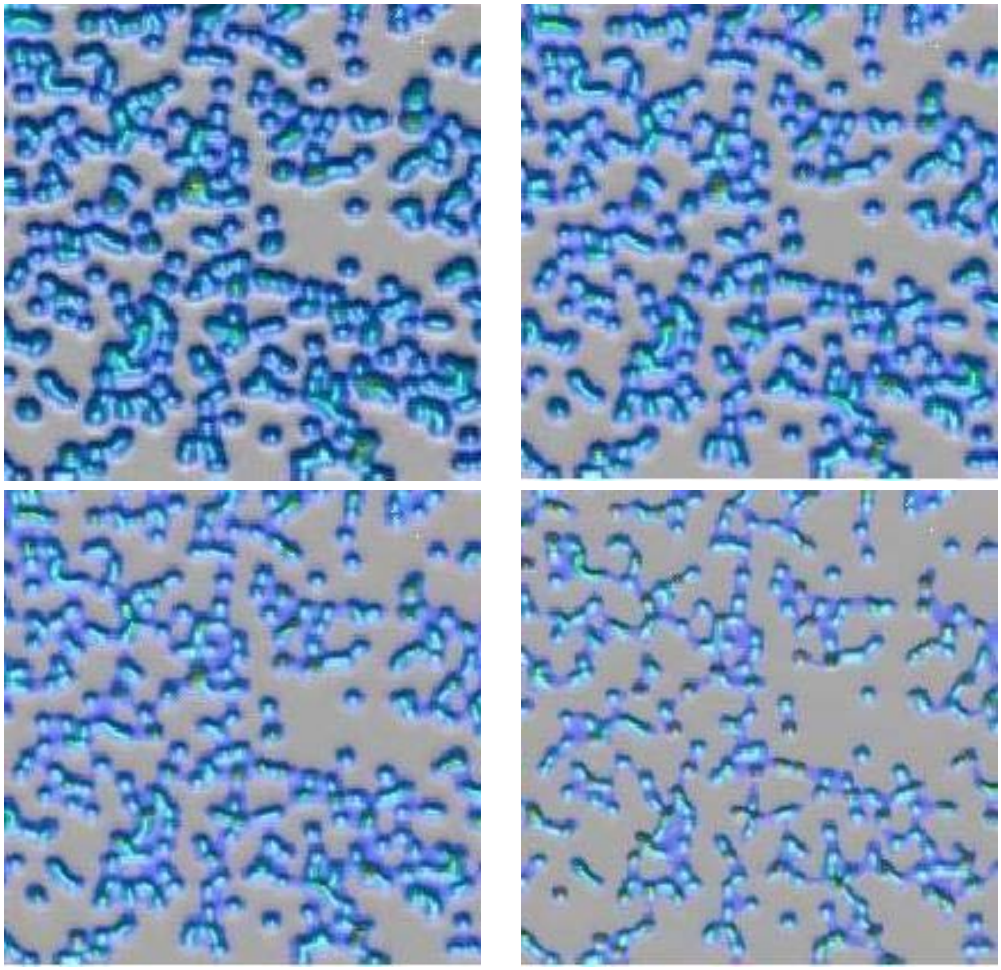

FIG. 7. *Formation of network: time evolution* ($t = 0.17$, 0.22, 0.26, *and* 0.42) *of the cell density with* $N = 800$.

results for longer time because the numerical solution blows up (cell concentrations become larger and larger), as is expected from theoretical results on other models (Euler–Poisson [14] or parabolic system PKS [9, 15]). But, the transient regime seems to be well described by the hyperbolic model. In this last example, we do not gain any advantage by using the well-balanced algorithm since the solution does not converge to a steady state, but even in this case the method works well.

REFERENCES

[1] E. AUDUSSE, F. BOUCHUT, M.-O. BRISTEAU, R. KLEIN, AND B. PERTHAME, *A fast and stable well-balanced scheme with hydrostatic reconstruction for shallow water flows*, SIAM J. Sci. Comput., 25 (2004), pp. 2050–2065.

[2] F. BOUCHUT, *Nonlinear Stability of Finite Volume Methods for Hyperbolic Conservation Laws and Well-balanced Schemes for Sources*, Birkhäuser, Basel, 2004.

[3] Y. DOLAK AND T. HILLEN, *Cattaneo models for chemotaxis, numerical solution and pattern formation*, J. Math. Biol., 46 (2003), pp. 461–478.

[4] F. Filbet, Ph. Laurençot, and B. Perthame, *Derivation of hyperbolic models for chemosensitive movement*, J. Math. Biol., 50 (2005), pp. 189–207.
[5] A. Gamba, D. Ambrosi, A. Coniglio, A. de Candia, S. Di Talia, E. Giraudo, G. Serini, L. Preziosi, and F. Bussolino, *Percolation, morphogenesis, and Burgers dynamics in blood vessels formation*, Phys. Rev. Lett., 90 (2003), 118101.
[6] L. Gosse, *Report on the Euler-Poisson Project*, CNR report, http://www-dimat.unipv.it/∼laurent/report.ps.gz (2000).
[7] L. Gosse and A.-Y. LeRoux, *A well-balanced scheme designed for inhomogeneous scalar conservation laws*, C. R. Acad. Sci. Paris Sér. I Math., 323 (1996), pp. 543–546 (in French).
[8] J. M. Greenberg and A. Y. Leroux, *A well-balanced scheme for the numerical processing of source terms in hyperbolic equations*, SIAM J. Numer. Anal., 33 (1996), pp. 1–16.
[9] M. A. Herrero, E. Medina, and J. J. L. Velázquez, *Finite-time aggregation into a single point in a reaction-diffusion system*, Nonlinearity, 10 (1997), pp. 1739–1754.
[10] T. Hillen and H. G. Othmer, *The diffusion limit of transport equations derived from velocity jump processes*, SIAM J. Appl Math., 61 (2000), pp. 751–775.
[11] T. Hillen, *Hyperbolic models for chemosensitive movement*, Math. Models Methods Appl. Sci., 12 (2002), pp. 1007–1034.
[12] G. Jiang and C.-W. Shu, *Efficient implementation of weighted ENO schemes*, J. Comput. Phys., 126 (1996), pp. 202–228.
[13] E. F. Keller and L. A. Segel, *Traveling band of chemotactic bacteria: A theoretical analysis*, J. Theoret. Biol., 30 (1971), pp. 235–248.
[14] T. Makino and B. Perthame, *Sur les solutions à symétrie sphérique de l'équation d'Euler-Poisson pour l'évolution d'étoiles gazeuses*, Japan J. Appl. Math., 7 (1990), pp. 165–170.
[15] A. Marrocco, *Numerical simulation of chemotactic bacteria aggregation via mixed finite elements*, M2AN Math. Model. Numer. Anal., 37 (2003), pp. 617–630.
[16] S. Osher, *Convergence of generalized MUSCL schemes*, SIAM J. Numer. Anal., 22 (1985), pp. 947–961.
[17] H. G. Othmer and T. Hillen, *The diffusion limit of transport equations* II: *Chemotaxis equations*, SIAM J. Appl. Math., 62 (2002), pp. 1222–1250.
[18] H. G. Othmer, S. R. Dunbar, and W. Alt, *Models of dispersal in biological systems*, J. Math. Biol., 26 (1988), pp. 263–298.
[19] C. S. Patlak, *Random walk with persistence and external bias*, Bull. Math. Biol. Biophys., 15 (1953), pp. 311–338.
[20] P. Roe, *Approximate Riemann solvers, parameter vectors and difference schemes*, J. Comput. Phys., 27 (1978), pp. 1–31.
[21] G. Serini, D. Ambrosi, E. Giraudo, A. Gamba, L. Preziosi, and F. Bussolino, *Modeling the early stages of vascular network assembly*, EMBO J., 22 (2003), pp. 1771–1779.
[22] C.-W. Shu, *Essentially non-oscillatory and weighted essentially non-oscillatory schemes for hyperbolic conservation laws*, in Advanced Numerical Approximation of Nonlinear Hyperbolic Equations, B. Cockburn, C. Johnson, C.-W. Shu, and E. Tadmor, eds., Lecture Notes in Math. 1697, Springer, New York, 1998, pp. 325–432.
[23] C.-W. Shu and S. Osher, *Efficient implementation of essentially non-oscillatory shock capturing schemes*, J. Comput. Phys., 77 (1988), pp. 439–471.
[24] C.-W. Shu and S. Osher, *Efficient implementation of essentially non-oscillatory shock capturing schemes*, II. J. Comput. Phys., 83 (1989), pp. 32–78.
[25] A. Stevens, *The derivation of chemotaxis equations as limit dynamics of moderately interacting stochastic many-particle systems*, SIAM J. Appl. Math., 61 (2000), pp. 183–212.